Electronic Supplementary Material (ESI) for Lab on a Chip.

Supplementary Materials

Programmable Assembly of Heterogeneous Microparts by an Untethered Mobile Capillary Microgripper

Joshua Giltinan[1,2], Eric Diller[3], and Metin Sitti[1,2,*]

[1]*Max-Planck Institute for Intelligent Systems, 70569 Stuttgart, Germany*

[2]*Department of Mechanical Engineering, Carnegie Mellon University, Pittsburgh, PA 15213, USA*

[3]*Department of Mechanical and Industrial Engineering, University of Toronto, Toronto, ON, M5S 3G8 Canada*

[*]*sitti@is.mpg.de*

Fabrication

Microgrippers

Single-cavity microgrippers for peel-off analysis For ease of fabrication and handling, all single-cavity microgrippers were given geometry of a 250 x 250 x 125 μm rectangular cuboid. These microgrippers were used to obtain the data for maximizing and minimizing the peel-off force. Microgrippers 5 and 6 were coated in perfluorodecyltrichlorosilane by chemical vapor deposition to increase the advancing contact angle of the material to $\sim$115°. Polymer master structures of the

microgrippers with detachment features are shown in Fig. S2 where defects from the two-photon lithography process can be seen.

Microgripper #	r (μm)	d (μm)	r/d	$\lvert\vec{m}\rvert$ (nAm^2)	L (μm)	SAM coating
1	25	100	0.25	382.8	222	no
2	25	55	0.45	258.4	221	no
3	75	100	0.75	250.2	245	no
4	75	55	1.36	326.4	218	no
5	75	55	1.36	395.0	225	yes
6	75	25	3	303.4	250	yes

Table S1: Microgrippers used for the study of the capillary attachment (SAM: self-assembled monolayer).

Microgripper #	microbump features	feature size (μm)	L (μm)	$\lvert\vec{m}\rvert$ (nAm^2)
7	4 cones	20	235	100.1
8	3 cones	20	223	101.3
9	5 cones	20	232	100.5
10	4 cones	10	226	99.7
11	4 hemispheres	20	227	100.7
12	none	n/a	216	100.3

Table S2: Microgrippers used for the comparison of different detachment minimization microbump protrusions.

Five-cavity microgrippers for assembly tasks Five cavities were placed on the microgripper to ensure a bubble will face the part as the microgripper approaches it in the z-direction, even if the bubble direction could not be oriented by open loop control. If fewer bubbles were present, then the bubbles would rotate the microgripper about the sixth, uncontrolled, degree-of-freedom to face upward, away from the object. The "sixth-DOF" in magnetic microrobot control is the orientation about the magnetization axis of the body, as this orientation cannot be open-loop controlled by the magnetic torque[1]. The sixth face is not given a cavity due to limitations of the soft lithography molding technique. We magnetize the microgripper such that this face is normal to the magnetization axis. A cube of 200 μm length was chosen for the demonstration due to two-photon lithography limitations at the time of design. Each face was given five equally distributed cones of 10 μm height and 20 μm radius to minimize surface contact with the manipulated object. A molded example is shown in Fig. 1G.

Manipulated parts

Kapton film Kapton film was cut from 25 μm thick sheet of Kapton HN Thermal Insulating Film (DuPont) using a precision laser mill (ProtoLaser U3, LPKF Laser & Electronics AG).

Hydrogels The Poly(ethylene glycol) diacrylate (PEGDA) hydrogels were fabricated by placing a droplet of 99% PEGDA (575 molecular weight) and 1% Irgacure 819 photoinitiator (Ciba Specialty Chemicals), mixed with drops of pigment (So-Strong, Smooth-On Inc.), onto a glass slide. For planar hydrogels, a photomask was placed on 100 μm thick spacers, and the solution was cross linked under 365 nm wavelength light for 30 seconds. The samples were then developed in water. Hydrogel spheres were fabricated by preparing a PDMS negative mold from glass spheres with diameters in the range of 212-300 μm (Sigma-Aldrich Co.). The molds were filled and a vacuum was applied to fill the molds, but not below the vapor pressure of water at room temparture. Excess material was carefully removed and the solution was cross linked as above.

Contact angle measurements

Contact angles of the parts and NdFeB/polyurethane material were measured using the sessile drop method by a Krüss Drop Shape Analyzer DSA100 and are given in Table S3.

water contact angle	advancing	receding
NdFeB/polyurethane composite	95°± 4°	57°± 1°
polyurethane (Smooth-Cast 310)	92°± 2°	48°± 1°
silicon	98°± 2°	50°± 1°
kapton	90°± 2°	53°± 3°
PEGDA (MW 515) hydrogel	22°± 3°	15°± 2°
Denatured pig muscle tissue	46°± 3°	43°± 3°
Hair	103° [2]	

Table S3: Measured contact angles of the materials used in experiments. The average values were used in finite element modeling.

Further Discussion of the Peel-off Results

Cacluating the experimental capillary attachment

The peel-off method was chosen as the maximum possible magnetic gradient force using the electromagnetic coil system described in the methods section, and is on the order of 1 μN: an order of magnitude lower than the capillary forces of interest. Magnetic torque scales more favorably with length, $\propto L^3$, compared to magnetic force, $\propto L^4$, and the coils are able to produce torques on the order of 20 nN·m, which are sufficient for detaching from the substrate. The microgripper is used as a pivot, and the achievable equivalent force is called the peel-off force. The equivalent peel-off force is given by

$$\left|\vec{F}_e\right| = \frac{2}{L}\left|\vec{m}\right|\left|\vec{B}\right|\sin\left(\theta_r\right), \tag{1}$$

where L is the microgripper length, θ_r is the rotation angle with respect to the horizontal ($\phi \to 0$) substrate, $\vec{B}$ is the magnetic field strength, and $\vec{m}$ is the magnetic moment of the microgripper. For microgrippers of length 250 μm, the maximum achievable equivalent force is roughly 200 μN. This method can be quickly and remotely used to approximate the attachment force of the bubble on the part.

Analysis of the picking peel-off force

The microgrippers, summarized in Table S1, were fabricated with cavities of 25 μm and 75 μm radii. Each was fabricated with depths of 55 μm and 100 μm. A microgripper with a 75 μm radius cavity was fabricated with a depth of 25 μm, but it was not able to reliably capture a bubble in each immersion. When coated with a hydrophobic self-assembled monolayer (SAM) coating, the capture repeatability was increased. A control microgripper with $r = 75$ μm and $d = 55$ μm was also prepared with the same SAM. The length of each microgripper, 250 μm, was kept constant within the limits of manufacturing precision of the polymer masters.

From Figure 4A, the p-value when performing Student's t-test on the microgrippers with 25 μm radius cavities is 0.0003, and the smallest p-value for the microgrippers with 75 μm radius cavities is 0.0046, between microgrippers with $d = 55$ μm and $d = 25$ μm. The p-value between the

identical microgrippers where only one has a SAM coating (marked with "*"), is 0.0207, and thus too ambiguous to make a meaningful statement on the effect the SAM may produce. However, the microgrippers with the larger cavity have a statistically significant larger peel-off force. When grouping microgrippers of the same cavity together and performing the t-test, the resulting p-value is 8.1×10^{-11}; therefore we group the cavities of equal radii together to yield more compact, significant, and meaningful results.

Analysis of the release peel-off force

A cone of 20 μm radius and 20 μm height was chosen as the primary microbump feature to enforce the minimum gap between the microgripper and the part. The first three microgrippers received these microbumps, which were placed onto microgrippers in a group of three, four, and five respectively. While the fewest contacts should yield the lowest adhesion between the microgripper and part, more microbumps would increase the probability that the minimum separation distance is enforced. The next microgripper received four cones at half the original height, 10 μm, as shorter cones would avoid unnecessary distance between the gripper and the part, but might have a greater chance to allow accidental contact. The final microbump design was a set of four hemispheres, as while conical microbumps more closely approximate single point contacts, spherical microbumps are more robust after molding; the tips of the cones were typically damaged after one to two experiments. These were compared to a control microgripper with no microbumps. All microgrippers were magnetized to a magnetization of 100.4 ± 0.5 nAm^2, with specific values given in Table S2 and the polymeric postive structures are shown in Fig. S2.

Assuming no electric charge buildup, the polished silicon surface is atomically smooth, and the point contacts have curvatures R_{vdW} on the order of $\sim$100 nm and are in full contact with the substrate, the adhesive van der Waals forces can be calculated by

$$F_{vdW} = \frac{A_{132}R_{vdW}}{6h^2}, \tag{2}$$

where the separation distance h is at full contact and approximated to the interatomic distance $a_0 \approx 0.17$ nm, and the Hamaker constant between silicon and polyurethane in water is calculated

to be approximately 20 zJ. With these values, the van der Waals forces are calculated to be on the order of 12 nN per microbump. Thus the difference between the adhesion of the microgripper with five microbumps and the microgripper with three microbumps should be 24 nN. The minimal differences between designs are considered negligible compared to the minimum observable $\left|\vec{F}_e\right|$ due to the electromagnet control algorithm, 70 nN for microgrippers with magnetization 100 nAm^2. The net weight of the microgripper, which so far has been neglected in the analysis, is approximately 200 nN (including buoyancy). This is similar to the $\left|\vec{F}_e\right|$ observed in Fig. 4G, and is an order of magnitude greater than the calculated van der Waals forces. Thus the results given are reasonable, and show that the weight of the microgripper, not adhesion, is dominating the peel-off force.

Bubble Volume Control Methods

Pressure

The pressure vessel used in this work was milled from aluminum. A hole in the bottom was connected to a 30 mL syringe pump, with a digital pressure gauge used to monitor ambient pressure (ACSI Model 1200 or Panasonic DP-111A-E-P). The pressure vessel is shown in Fig. S3A. The maximum pressure difference was limited by the syringe volume and initial plunger position, and was capable of at least ± 50 kPa relative to ambient pressure.

Temperature

To show the possibility of remote manipulation of objects using temperature, the microgripper workspace was removed from the pressure chamber and placed onto a Peltier device, which under an applied voltage will generate a temperature difference. The setup is shown in Fig. S3B. The current was set to an arbitrary 0.6 A during heating. The current was constantly increased during cooling to keep the temperature 4° below ambient temperature.

Calculation of the saturation constant

The gas itself, the ambient air, is assumed to be composed of 21% oxygen and 79% nitrogen for simplicity of calculation. The concentration of each are thus given by

$$c = H_{cp} p, \tag{3}$$

where H_{cp} is the Henry solubility, 76.67 kPa/(mol/liter) for oxygen and 162.12 kPa/(mol/liter) for nitrogen, and p is the partial pressure of the gas in equilibrium. This yields an oxygen solubility of 0.0089 g/kg and nitrogen solubility of 0.0138 g/kg. The sum of the solubility is thus the saturation concentration used in Figure 5, 0.023 g/kg.

Discussion of the effect of temperature on diffusion

When temperature control of the bubble volume is used, a complex scenario arises. The saturation concentration has a nonlinear dependency on temperature. In general, the Henry solubility perturbs about temperature based on the constant at standard conditions, H_o, by

$$H_{cp}(T) = H_o \, e^{\frac{-\Delta_{sol}H}{R}\left(\frac{1}{T}-\frac{1}{T_o}\right)}, \tag{4}$$

where $T_o = 298.15$ K, and $\frac{-\Delta_{sol}H}{R}$ is a tabulated value for the enthalpy of dissolution (-11.7 kJ/mole for O_2).[3] For the example in Fig. S3D, the saturation concentration changes in a manner as if the pressure was changed by -36 kPa. This is even greater than the pressure used in Fig. 5B, and so may have contributed to the bubble change seen in Fig. S3D. The calculation of diffusivity also changes with temperature, T, as well, and can be approximated by the Stokes-Einstein equation,

$$\kappa = \frac{k_b T}{3\pi D_m \mu}, \tag{5}$$

where k_b is the Boltzmann constant, D_m is the average molecular diameter of air, ~ 1.8 Å, and μ is the dynamic viscosity of water, 8.9×10^{-4} Pa $\cdot$ s at room temperature (and which varies with temperature).[4,5] The resulting change is not as important as that on the Henry solubility, but is

noted for completeness.

If localized heating is used, then the temperature of the liquid will depend on the gripper's position, duration at that position, and heat dissipation. All of these effects are application specific, and would require complex modeling of the system beyond the scope of this work. However, it might indicate that the overall time varying effects may be limited if the heat is directly applied to the bubble.

Force-Separation Curves

The Surface Evolver allows us to analyze cases that could not be experimentally tested due to challenges of the experimental setup. In particular, we are interested in the force-separation curves for various microgrippers and parts, showing the capillary force in the z-direction between them for a given separation in the z-axis. Example force-separation curves are given in Fig. S4A for a bubble height of 50 μm for both 25 and 75 μm cavities.

Figure S4B shows the effect of changing the bubble height on the adhesion between a microgripper and the silicon substrate. The cavity radii of 25 and 75 μm are used again, and the trends follow those of Fig. 4B. However, the force magnitudes are generally larger than the peel-off forces.

While the force-separation here curves are calculated by the Surface Evolver, analytical methods for calculating the capillary force have been shown assuming the mean curvature of the capillary bridge is constant. These have been shown to agree with Surface Evolver calculations for small separations between plates.[6]

Media

Movie 1. The stacking of two planar hydrogels, corresponding to Fig. 7F-M, and the manipulation of the various parts, corresponding to Fig. 7A-E.

References

[1] E. Diller, J. Giltinan, G. Z. Lum, Z. Ye and M. Sitti, *Int. J. Rob. Res.*, 2016, **35**, 114–128.

[2] R. Molina, F. Comelles, M. R. Juliá and P. Erra, *J. Colloid Interface Sci.*, 2001, **237**, 40–46.

[3] R. Sander, *Atmos. Chem. Phys.*, 2015, **15**, 4399–4981.

[4] E. L. Cussler, *Diffusion: mass transfer in fluid systems*, Cambridge University Press, 2009.

[5] L. Liebermann, *J. Appl. Phys.*, 1957, **28**, 205–211.

[6] E. De Souza, M. Brinkmann, C. Mohrdieck, A. Crosby and E. Arzt, *Langmuir*, 2008, **24**, 10161–10168.

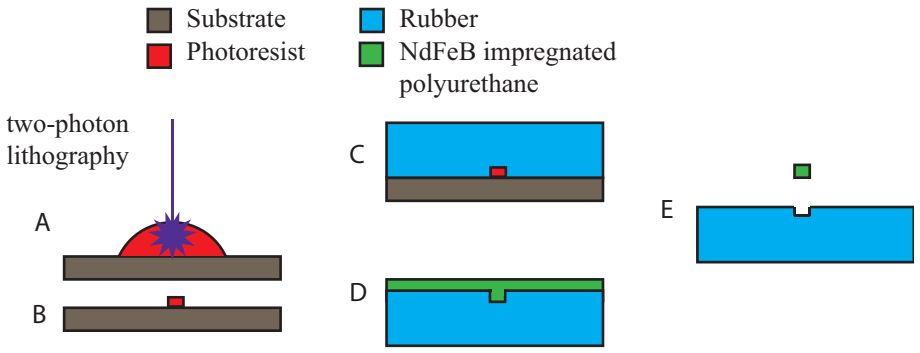

Fig. S1: **Fabrication of microgrippers.** (**A**) Creation of postive mold using 3D lithography and (**B**) removal of excess photoresist. (**C**) Negative mold of the master. (**D**) NdFeB particles in liquid polyurethane are placed in the mold. (**E**) Cured microgripper is removed.

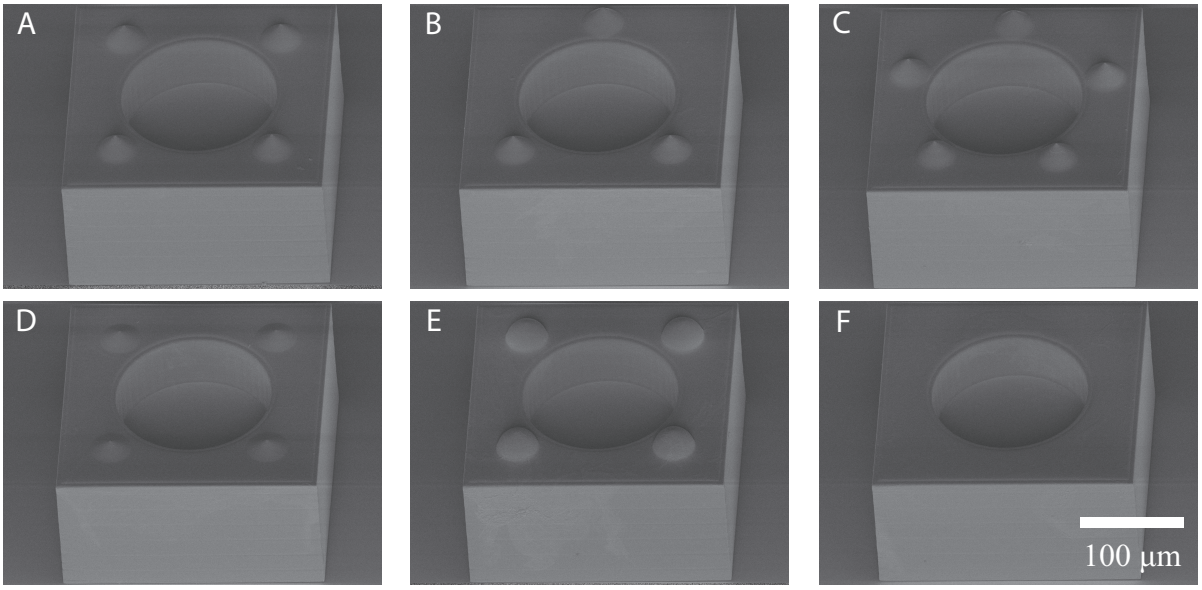

Fig. S2: **Microgripper polymer positive structures with detachment features from Table S2.** (**A-E**) correspond to microgrippers 7-12, respectively. Minor defects due to two-photon lithography are assumed to be negligible.

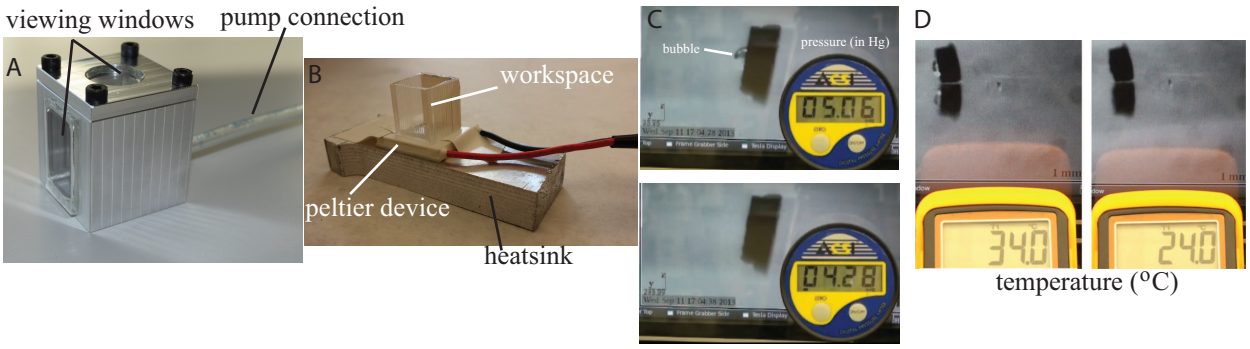

Fig. S3: **Bubble control methods and results.** (**A**) Pressure vessel used to encapsulate the microgripper workspace. The syringe pump used to manually apply the pressure difference is not shown. (**B**) Peltier setup to apply a temperature difference to the workspace. The aluminum heatsink is required for the cooling of the workspace. (**C**) Results of applied pressure differences in a short time scale (corresponding to Fig. 5A). The applied pressure difference is given in inches of mercury. (**D**) Results of applied temperature difference. Room temperature was recorded to be 27°C. There is a delay in the recorded temperature and the microgripper response. The workspace was heated to 50°C and then cooled to 22°C. The elapsed time was on the order of 10 minutes due to the slow heat dissipation in cooling through the aluminum heatsink.

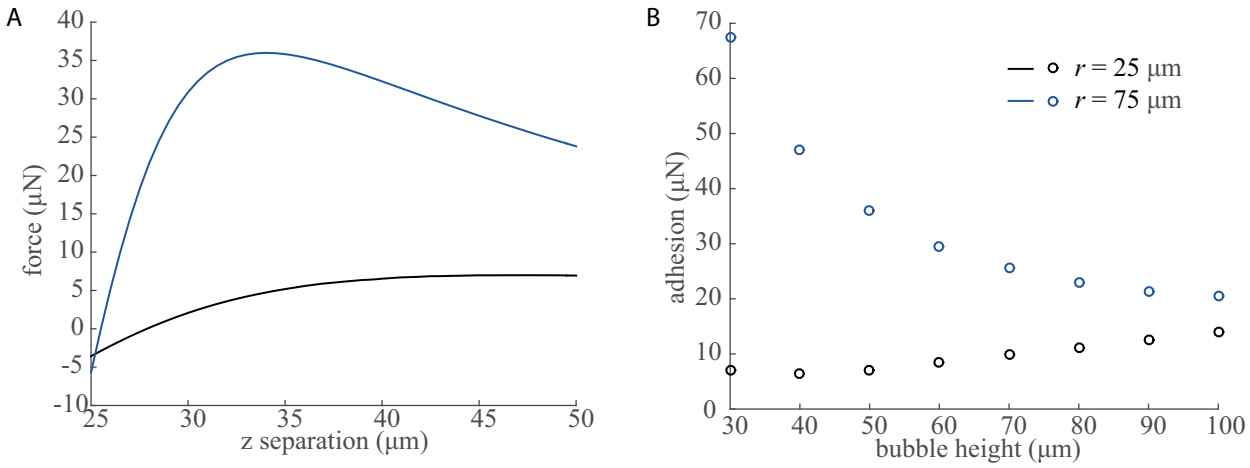

Fig. S4: **Force separation curve examples.** (**A**) Force-separation curve for the experimental conditions used in Fig. 4 with $h = 50$ μm. (**B**) Adhesion with respect to the bubble height. The trends are similar to those seen in Fig. 4B.